How does hemodynamics affect rupture tissue mechanics in abdominal aortic aneurysm: Focus on wall shear stress derived parameters, time-averaged wall shear stress, oscillatory shear index, endothelial cell activation potential, and relative residence time

Onur Mutlu [a], Huseyin Enes Salman [b], Hassan Al-Thani [c], Ayman El-Menyar [c,d], Uvais Ahmed Qidwai [e], Huseyin Cagatay Yalcin [a,*]

[a] Biomedical Research Center, Qatar University, Doha, Qatar
[b] Department of Mechanical Engineering, TOBB University of Economics and Technology, Ankara, Turkey
[c] Department of Surgery, Trauma and Vascular Surgery, Hamad General Hospital, Hamad Medical Corporation, P.O. Box 3050, Doha, Qatar
[d] Clinical Medicine, Weill Cornell Medical College, Doha, Qatar
[e] Department of Computer Science Engineering, Qatar University, Doha, Qatar

ARTICLE INFO

ABSTRACT

An abdominal aortic aneurysm (AAA) is a critical health condition with a risk of rupture, where the diameter of the aorta enlarges more than 50% of its normal diameter. The incidence rate of AAA has increased worldwide. Currently, about three out of every 100,000 people have aortic diseases. The diameter and geometry of AAAs influence the hemodynamic forces exerted on the arterial wall. Therefore, a reliable assessment of hemodynamics is crucial for predicting the rupture risk. Wall shear stress (WSS) is an important metric to define the level of the frictional force on the AAA wall. Excessive levels of WSS deteriorate the remodeling mechanism of the arteries and lead to abnormal conditions. At this point, WSS-related hemodynamic parameters, such as time-averaged WSS (TAWSS), oscillatory shear index (OSI), endothelial cell activation potential (ECAP), and relative residence time (RRT) provide important information to evaluate the shear environment on the AAA wall in detail. Calculation of these parameters is not straightforward and requires a physical understanding of what they represent. In addition, computational fluid dynamics (CFD) solvers do not readily calculate these parameters when hemodynamics is simulated. This review aims to explain the WSS-derived parameters focusing on how these represent different characteristics of disturbed hemodynamics. A representative case is presented for spatial and temporal formulation that would be useful for interested researchers for practical calculations. Finally, recent hemodynamics investigations relating WSS-related parameters with AAA rupture risk assessment are presented. This review will be useful to understand the physical representation of WSS-related parameters in cardiovascular flows and how they can be calculated practically for AAA investigations.

1. Introduction

Aorta is the largest blood vessel in the body, transporting the blood from the heart to the body's other organs at high pressure and velocity. Unexpected abnormalities or disorders that may occur in the aorta can lead to major health problems in the circulatory system or even death. Between 1990 and 2010, the global death rate from aortic diseases increased from 2.49 to 2.78 per 100,000 of the population worldwide [1, 2]. One of the most prevalent aortic disorders is aortic aneurysm, which is caused by abnormal balloon-shaped aortic enlargement. The term abdominal aortic aneurysm (AAA) refers to an aortic dilatation that exceeds 50% of the normal vessel diameter [3]. According to the reports, 4–8% of males and 0.5–1% of women over the age of 50 have an AAA, which accounts for 15,000 fatalities each year in the United States alone [4,5]. The aforementioned incidence rates indicate the critical importance of early diagnosis and health care for AAAs.

The majority of people with non-ruptured aneurysms normally have no symptoms. Unfortunately, over 75% of patients do not show clinical

---

signs of an imminent AAA rupture [6]. Particularly in patients with coronary, peripheral, or cerebrovascular disorders, AAAs are detected by chance or during a thorough clinical examination carried out for general health screening [7]. In rare cases, the problems including distal embolization and acute thrombosis might lead to the diagnosis of non-ruptured aneurysms [4].

AAA rupture can lead to a deadly surgical emergency condition, mainly due to hematocele and decreased blood supply to essential organs. AAA rupture is the most severe consequence of aneurysmal disease, with an astonishing overall death rate of 80%. Since the majority of ruptured aneurysms never reach the stage of a surgical operation, ruptured AAA operations are known to only be the tip of the iceberg. Although there have been reports of improved operational results for ruptured AAAs, overall mortality is still high and further advancements only have a limited impact [8]. Therefore, early and appropriate care for AAA detected by medical imaging modalities will significantly reduce the risk of rupture and mortality rates.

A convenient rupture risk assessment of AAA has a critical importance for early warning. The standard clinical practice is to refer patients with large AAAs (diameter >5.5 cm) for surgical repair [9]. If the AAA growth rate is greater than 1 cm/year, this condition is also evaluated as a high-risk factor, and surgical repair is recommended depending on the general health status and life expectancy of the patient. For relatively smaller AAAs (diameter <5.5 cm), regular monitoring with ultrasonography is provided, and patients are referred for surgery if the aneurysm diameter reaches 5.5 cm or larger, or if the growth rate exceeds 1 cm/year [10,11]. It should be noted that the aneurysm diameter criterion provides a rough estimate of the case and is not always accurate in terms of rupture risk identification. Although surgical intervention is performed for large AAAs and regular monitoring of small diameter aneurysms is recommended, there are exceptional cases where 9 cm diameter AAAs may remain stable [12] and AAAs smaller than 5.5 cm may rupture [13–17]. No matter how small the aneurysm is, approximately 70% of AAAs will need to be surgically repaired within 10 years of the first diagnosis, depending on the rate of growth [18]. As a consequence, monitoring the diameter of the aneurysm with simple medical imaging techniques may be insufficient to intervene in the AAA at the appropriate time before it ruptures.

The rupture can be defined as the mechanical failure of the aorta due to the weakening of the arterial structure. The degeneration of the pathological structure, such as the elastic fibrin and collagen fibers in the aorta, is known to reduce the strength of the arterial wall, which leads to AAA. On the other hand, pathological degeneration is not sufficient to produce an abnormal balloon shape. The development of such abnormal structures is caused by the dynamic effect of high pressure and flow velocity in the aorta in addition to the weakened arterial wall. The luminal and endothelial wall surfaces of arteries are constantly subjected to wall shear stress (WSS) as a result of the hemodynamic effects of the blood flow. WSS is caused by the frictional component of the flow-driven hemodynamic forces on the arterial wall. In numerous studies, it has been demonstrated that shear stress has a direct impact on vessel wall remodeling [19–21]. The cumulative result of the endothelium-mediated compensatory reactions is to keep the mean arterial hemodynamic shear stress between 15 and 20 dyn/cm^2 [22]. Therefore, the deterioration of the healthy endothelium structure and the non-stabilized shear stresses acting on the vessel wall resulting in the formation of abnormal structures on the vessel surface. In addition to the frictional effects of WSS, normal pressure and circumferential stretch also play a role in tissue degeneration. To summarize, AAA formation and rupture occur when the blood flow-driven stresses acting on the aneurysm exceed the limits of wall tissue strength. Therefore, the determination of hemodynamic effects and blood flow profiles in AAA are crucial for performing an accurate rupture risk assessment. According to the hemodynamic simulations, the majority of ruptured aneurysms displayed complex flow patterns with several independent flow vortices. Contrarily, the majority of non-ruptured aneurysms resulted in relatively simpler flow patterns with a single vortex [23].

Doppler Ultrasound and flow MRI are the most commonly used clinical imaging modalities for studying the flow hemodynamics in major vessels [24–28]. In Doppler ultrasound, the velocity of moving red blood cells is calculated from the frequency shift of the sound echo signal [29]. This technique can provide an average flow velocity in a 2-D vessel cross-section. In flow MRI, the flow velocity is obtained using the changes in the MR signal phase along a magnetic field gradient [30]. This technique can be used for 3D velocity measurement for vessel volume. Another approach for studying cardiovascular hemodynamics is computationally calculating the complex stresses on aneurysmal tissue. Particularly, the computational fluid dynamics (CFD) approach enables investigation of the disturbed hemodynamics and frictional shear stresses acting on vessel walls. Here, governing physical equations are solved using patient-specific blood flow and geometry information as boundary condition input. CFD simulations would give detailed information for the fluid field of study making it very useful to study particularly unsteady flows such as cardiovascular flows. Velocity gradients near the wall can be calculated accurately, enabling assessing wall shear stress in the boundary layer. CFD techniques have been applied extensively to investigate complex flow patterns in the aorta [31–33], and several other studies have tried to link hemodynamic parameters from CFD with the AAA progression and eventual rupture risk [19,21,34–38]. The application of CFD for the prediction of AAA rupture risk has been reviewed elegantly in some recent review papers [3,19,39, 40]. In a few pioneering clinical investigations, a patient-specific CFD approach has been adapted for surgery planning of AAA patients and has shown great promise [40]. Such computational approaches will most likely be the most powerful way of predicting AAA rupture risk in near future, however, these are still not very practical and readily available to be adapted to clinical practice, and validation of these tools remains a significant challenge [3,41].

CFD analysis identifies and quantifies the wall shear stresses that develop within the aneurysm wall, assisting surgeons in determining whether surgical intervention is required. However, to accurately estimate the stresses that develop in the AAA wall, the mechanical effect of hemodynamic forces on the AAA wall must be understood. The new approach is based on fluid-structure interaction (FSI) analysis, which allows the evaluation of both the hemodynamic forces of blood flow and the mechanical stresses acting on the AAA wall. The FSI analysis can assess the effect of the rupture caused by wall shear stress and the enlargement of the aneurysm diameter [34,42,43]. Furthermore, calculating the static uniform pressure on the AAA surface to determine the rupture region yields more precise and sensitive results than the maximal diameter, which is utilized as the sole tear risk factor [44,45]. The effects of mechanical stress produced by hemodynamic forces on variations in aneurysm wall thickness were investigated in FSI studies using idealized aneurysm geometries with different wall thicknesses, and it was determined that including ILT in the aneurysm, geometries will give more accurate results [46]. Consequently, it was discovered that variations in wall thickness cause higher stresses and increase the risk of rupture when compared to models with uniform wall thickness, and it was discovered that ILT can significantly reduce the stress on the wall [47–50].

Another important point is the challenges in characterizing unsteady disturbed flows with an AAA. WSS-related hemodynamic parameters, such as time-averaged WSS (TAWSS), oscillatory shear index (OSI), endothelial cell activation potential (ECAP), and relative residence time (RRT) are useful to evaluate the complex shear environment affecting the AAA wall. Some recent computational studies made a substantial contribution in that field to adapt the CFD approach in the rupture risk assessment of AAAs, in line with the flow chart in Fig. 1. Here researchers tried to relate characteristics of disturbed flows with AAA rupture locations (Table 1). Calculation of these parameters is not straightforward and requires a physical understanding of what they represent. In addition, CFD solvers do not readily calculate these
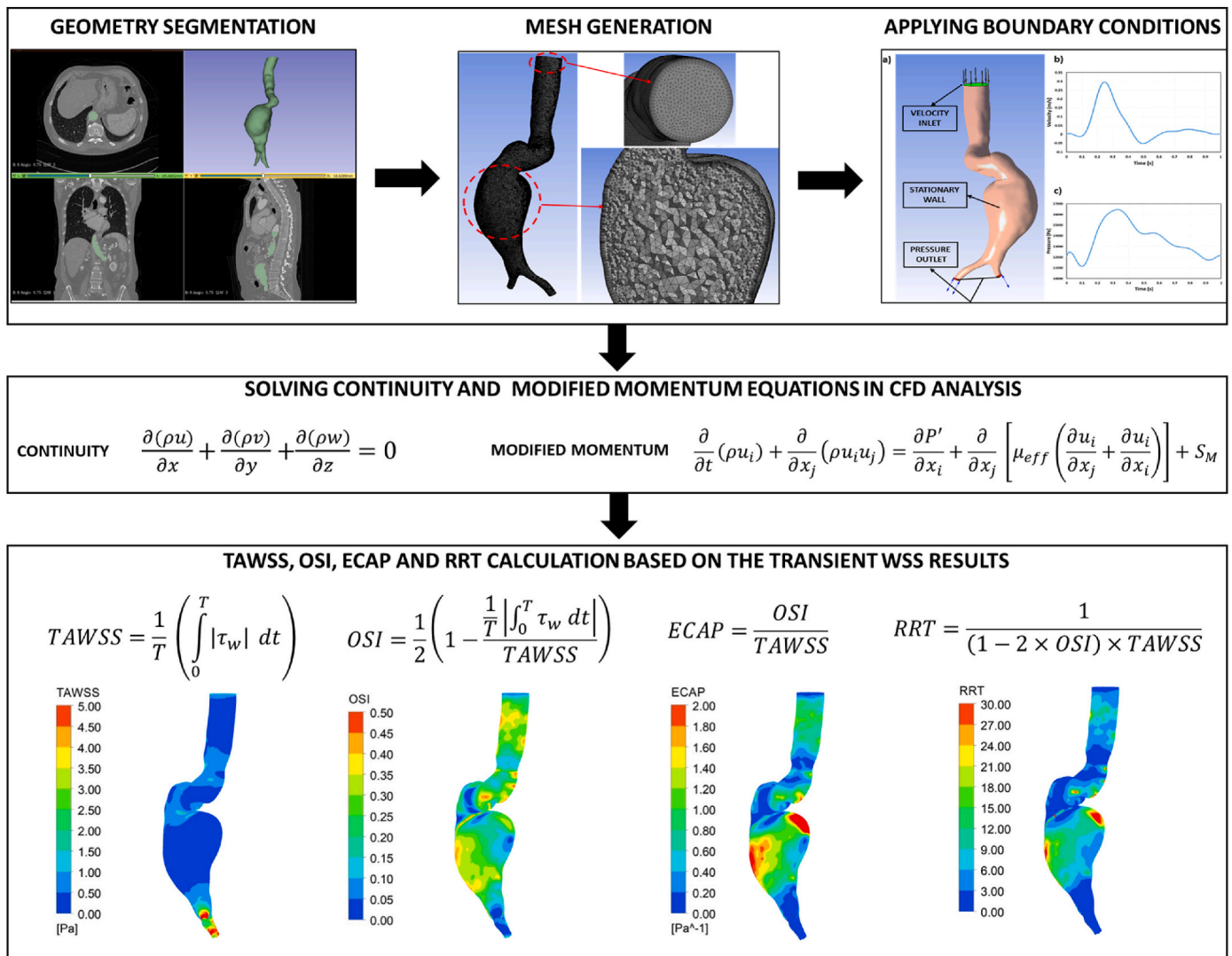
Fig. 1. The most prevalent methods for investigating disrupted hemodynamics, WSS, and WSS-derived parameters for AAA rupture.

parameters when hemodynamics is simulated. Therefore, investigating AAA rupture risk with hemodynamic parameters is challenging.

This review aims to explain the WSS-derived parameters focusing on how they represent different characteristics of disturbed hemodynamics. A representative case is presented for spatial and temporal formulation that would be useful for interested researchers for practical calculations. Finally, recent hemodynamics investigations relating WSS-related parameters with AAA rupture risk assessment are presented. This review will be useful to understand the physical representation of WSS-related parameters in cardiovascular flows and how they can be calculated practically for AAA investigations.

2. AAA (Abdominal aortic aneurysm) hemodynamics

The aorta is the largest artery in the human body, which is directly attached to the heart. It carries the majority of the blood in the body and ensures that an adequate amount of blood is distributed throughout the entire vascular system [60]. Hence, the aorta is subjected to high levels of mechanical stress because of the high-pressure blood flow that is pumped from the heart. The high-velocity flow in the aorta also results in high WSS levels which directly affect the vascular wall and lead to abnormalities in the vascular function [61]. Theoretically, WSS in the internal flows can be calculated by finding the tangential force per unit wall area, which is directly proportional to the velocity gradient. WSS

levels are expected to be high if the velocity gradient is high near the wall. On the other hand, lower flow velocities will result in lower WSS because of the low-velocity gradient near the wall, but this condition will also increase the blood residence time near the arterial wall. In most cases, the WSS levels of the post-aneurysm aorta are frequently higher than that of the pre-aneurysm aorta [62].

The hemodynamic conditions in the aorta change substantially along its length, from a high Reynolds Number value at the aortic root to low and oscillatory shear values at the aortic bifurcations [63]. In Fig. 2, the blood flow dynamics in normal, non-ruptured, and ruptured AAAs are compared to a healthy abdominal aorta. As can be seen in the comparison, the flow velocity decreases in the aneurysm sac due to the enlargement of the vessel, which leads to a recirculating flow pattern. In the healthy aorta, the flow velocities have a relatively homogenous distribution throughout the cardiac cycle compared to AAA flow. It can be concluded that a heterogeneous hemodynamic environment is produced in AAAs, one as a disturbed recirculating flow with low and oscillating WSS, and the other as a flow with a high WSS gradient (WSSG) [64–72]. The remodeling of developing and mature arteries is significantly influenced by these flow variables of local hemodynamics in both healthy and pathological conditions [73].

Besides the flow conditions, the blood flow hemodynamics are impacted by changes in vessel volume and shape. Accordingly, it has been demonstrated that hemodynamic variables in AAAs, such as

Table 1
Previous CFD studies where the correlation of WSS-derived parameters and AAA rupture locations were investigated.

Reference	Investigated WSS parameters based on CFD results	Remarks
Forneris et al., 2020 [51]	TAWSS	Aneurysm rupture associated with low TAWSS and thick thrombus deposition
Doyle et al., 2014 [52]	TAWSS	The AAA ruptured in the proximal, low TAWSS zone where the flow was recirculating.
McClarty et al., 2021 [53]	WSS magnitude at peak systole	The rupture occurred in a low WSS zone and was related to a significant increase in AAA diameter from 6.6 to 8.4 cm.
Qiu et al., 2019 [54]	TAWSS, OSI, ECAP	Without an ILT in the sac, the rupture was correlated with extremely low WSS and high ECAP.
Boyd et al., 2016 [55]	WSS magnitude	The rupture occurred in locations with low WSS and ILT deposition.
Boniforti et al., 2021 [56]	TAWSS, OSI	AAA rupture is related to high ILT deposition, low TAWSS, and high OSI values.
Qiu et al., 2018 [35]	WSS	All of the rupture locations were in stagnation zones with near-zero wall shear stress (WSS) but a high WSS gradient (WSSG).
Xenos et al., 2010 [34]	WSS	The ruptured AAAs have near-zero WSS values on the aneurysm sac compared to normal and non-ruptured aneurysms.
Arzani et al., 2014 [57]	TAWSS, OSI	The rate of thrombus growth may be a predictor of rupture. High OSI (>0.4) and very low TAWSS (1 dyn/cm2) locations did not appear to encourage thrombus deposition.
Trenti et al., 2022 [58]	RRT	Increasing RRT along the artery wall may promote the absorption of inflammatory cells and biomarkers, contributing to aortic wall degradation that leads to enlargement and rupture.
Doyle et al., 2014 [52]	TAWSS	Areas of low TAWSS correspond with lumen expansion and ILT formation. During the rapid expansion (9 mm/year) period preceding rupture, the proximal lobe of the lumen exhibited low TAWSS.
Teng et al., 2022 [59]	WSS	Patients with a significant value of diameter, curvature, and a low WSS were identified as being at high risk of rupture.

velocity, vorticity, WSS, and turbulence intensity are patient-specific and vary from patient to patient [57,74–76]. Due to the structural differences, unique curved shapes, and varying diameters in patient-specific AAAs, each AAA case should be investigated individually. In areas with fusiform shapes, the reverse flow is more noticeable, and the blood flow velocity and oscillating WSS are several times lower than in healthy aortas [64]. Saccular AAAs display completely different hemodynamic circumstances, in which the blood is nearly stagnant within the aneurysm sac and wall flow parameters are similar to those of normal aortas [77].

Another important condition that affects AAA hemodynamics is the presence of an intraluminal thrombus (ILT). The layer of ILT reduces the flow volume inside the aneurysm sac. For a reliable hemodynamic investigation, the presence and thickness of ILT should be taken into account during the modeling stage of the AAA. The level of ILT significantly affects the hemodynamics as a result of the new flow volume caused by the ILT deposition [43]. In addition to the aforementioned factors affecting the AAA hemodynamics, the shape of the vascular structures around the aneurysm and the flow characteristics in these

structures directly affect the flow dynamics within the aneurysm [78–81].

2.1. Governing equations and CFD (Computational fluid dynamics) methodology

The flow variables are determined using the Continuity and Navier-Stokes Momentum equations as given in Eq. (1) and Eq. (2), respectively [82]. In these equations, v denotes the velocity vector, ρ_f denotes the mass density of the fluid, τ_f denotes the fluid stress tensor, and f_B denotes the body forces such as the gravity. For the incompressible flows, the continuity equation guarantees that the inlet and outlet mass flow rates are equal in the flow domain.

$$\nabla \bullet v = 0 \tag{1}$$

$$\rho_f \frac{dv}{dt} + \rho_f v \bullet \nabla v - \nabla \bullet \tau_f = f_B \tag{2}$$

The fluid stress tensor (τ_f) can be defined in terms of the fluid pressure (p) and the dynamic viscosity (μ) of the fluid as provided in Eq. (3) [82]. The term δ_{ij} denotes the Kronecker delta, and ε_{ij} denotes the strain rate of the fluid. The strain rate (ε_{ij}) can be defined in terms of the velocity vector (v) as given in Eq. (4).

$$\tau_f = -p\delta_{ij} + 2\mu\varepsilon_{ij} \tag{3}$$

$$\varepsilon_{ij} = \frac{1}{2}\left(\nabla v + \nabla v^T\right) \tag{4}$$

For the Newtonian fluids, the dynamics viscosity is constant and does not vary with the flow conditions. On the other hand, non-Newtonian fluids such as blood have a varying viscosity which changes depending on the local shear rate in the flow domain [32,33]. The non-Newtonian behavior of blood is particularly observed in the small arteries. For large arteries such as the aorta, the shear strain rate is above 50 s^{-1} and the changes in the dynamic viscosity of the blood can be neglected [83,84].

One of the ways to solve the governing flow equations is to use computational fluid dynamics (CFD) analysis. In the computational method, the flow domain is discretized into a finite number of spatial elements, which is known as meshing. The physical equations are then solved at each element of the mesh within the interested range of time intervals using appropriate time steps. Therefore, the method relies on the discretization of the problem in time and spatial domains. At this point, the boundary conditions have the utmost importance, and they must be determined realistically. The general approach is to isolate the interested region of the flow geometry by applying the inlet and outlet boundary conditions as prescribed velocity and pressure profiles that are changing with time. The no-slip condition is a commonly used boundary condition on the walls, which guarantees that the flow velocity is zero on the wall boundaries. After determining the solution, the flow variables such as the velocity, pressure, and WSS can be determined within the entire flow geometry. In a recent review paper, we explained in detail the flow hemodynamics within AAA and how to study these phenomena via experimental and computational techniques [19].

3. Critical hemodynamic parameters

Among the flow variables, WSS has particular importance in AAA flow simulations, because the endothelial cells on the arterial wall sense the level of WSS and regulate the remodeling of the artery according to the WSS levels [20]. Abnormal levels of WSS would lead to the deterioration of the arterial structure in the long term and may lead to the rupture of AAA. Therefore, WSS-related hemodynamic parameters have a prior interest in this study. The WSS-related parameters can be listed as a time-averaged wall shear stress (TAWSS), oscillatory shear index (OSI), endothelial cell activation potential (ECAP), and relative
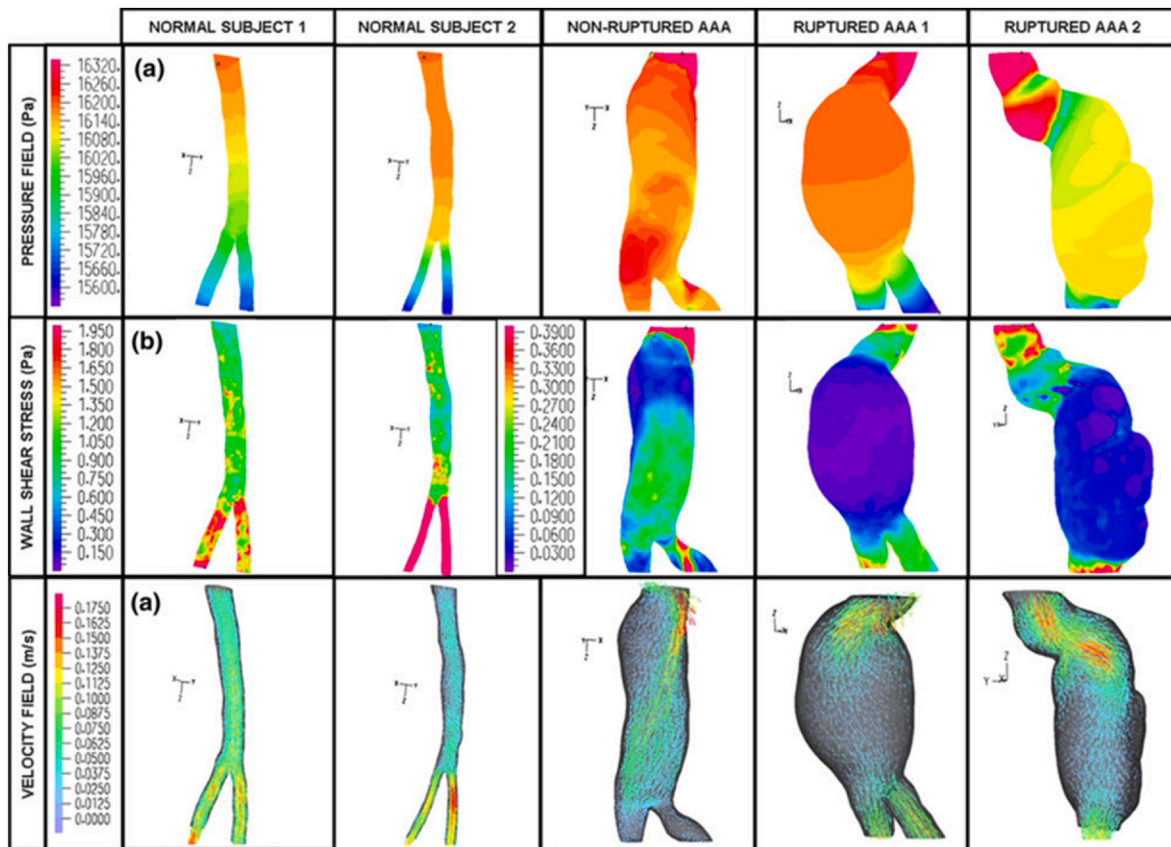
Fig. 2. The hemodynamic comparison of a non-ruptured and ruptured AAA with a healthy aorta. The figure is adapted from Ref. [34] and used with permission.

residence time (RRT). The following sections describe the methods for calculating the WSS-related parameters and explain how these parameters can be used in the rupture risk assessment of AAA.

3.1. TAWSS (Time-averaged wall shear stress)

TAWSS is a key parameter for detecting the critical locations on AAA which are prone to rupture as shown in Fig. 3. In the given figure, a retrospective analysis is performed using patient-specific images and TAWSS levels are provided around the ruptured locations of the investigated AAAs. It is observed that the rupture location cannot be determined directly by only quantifying the TAWSS levels, and other parameters such as the thickness of ILT also play a role in the rupture mechanism.

The formulation of TAWSS is defined in Eq. (5). For calculating TAWSS, the absolute values of x, y, and z components of WSS are used within the time period of T. In the general approach, the time period (T) is used as one full cardiac cycle. In Eq. (5), τ_w defines the instantaneous WSS vector.

$$\text{TAWSS} = \frac{1}{T}\left(\int_0^T |\tau_w| dt\right) \tag{5}$$

In many CFD analysis software packages, TAWSS formulation is not defined in the default post-processing options. Therefore, these analysis tools cannot directly calculate the TAWSS values at each mesh point. To determine the TAWSS distribution on AAA, the values of WSS vectors in three spatial dimensions (WSSx, WSSy, and WSSz) should be obtained at each time step, and then Eq. (5) should be implemented using an external software package (Matlab, Python, etc.).

For further clarification, a sample case can be considered for a 3D transient analysis with a cardiac cycle length of 1 s and time step size of 0.01 s (Total analysis time = 1 s, Time step size = 0.01 s, Cardiac cycle

length = 1 s). Each element on the AAA wall will yield WSSx, WSSy, and WSSz values at each time step (from time step 1 to 100). At each element, 100 WSSx, 100 WSSy, and 100 WSSz values will be obtained for the given example. If there are 2000 mesh nodes on the wall of the analyzed AAA geometry, the data can be summarized as presented in Table 2.

In the first step of TAWSS calculation, the WSS magnitude ($|\tau_w|$) should be calculated for each element and time step as given in Eq. (6), where the subscript k defines the time step number and n defines the element number on the AAA wall.

$$|\tau_w|_{k,n} = \sqrt{\left(WSSx_{k,n}\right)^2 + \left(WSSy_{k,n}\right)^2 + \left(WSSz_{k,n}\right)^2} \tag{6}$$

If $|\tau_w|_{1,1}$ (WSS magnitude of the first element at the first-time step) is calculated using the sample data provided in Table 2, the following equation will be obtained as given in Eq. (7).

$$|\tau_w|_{1,1} = \sqrt{(0.61)^2 + (0.42)^2 + (0.12)^2} = 0.750 \tag{7}$$

The WSS magnitude can be determined independently for each element, as shown in Table 3.

The TAWSS formulation given in Eq. (5) can be written in the form of Eq. (8) considering the temporally discretized results of CFD simulations. The integral operation is replaced by the summation of results at all time steps. In Eq. (8), TAWSS_n defines the TAWSS value for the element number n, T_k defines the total number of time steps within one full cardiac cycle, Δt defines the time step size, and $|\tau_w|_n$ defines the magnitude of instantaneous WSS for the element number n. In the previously given sample case, the cardiac cycle length is assumed as 1 s (T = 1 s) and the step size is used as 0.01 ($\Delta t = 0.01$ s), corresponding to 100-time steps with one cardiac cycle ($T_k = 100$). For the sample case, TAWSS_n can be directly found by summing all the WSS values and then dividing by 100 as shown in Eq. (8). The procedure is applied for each
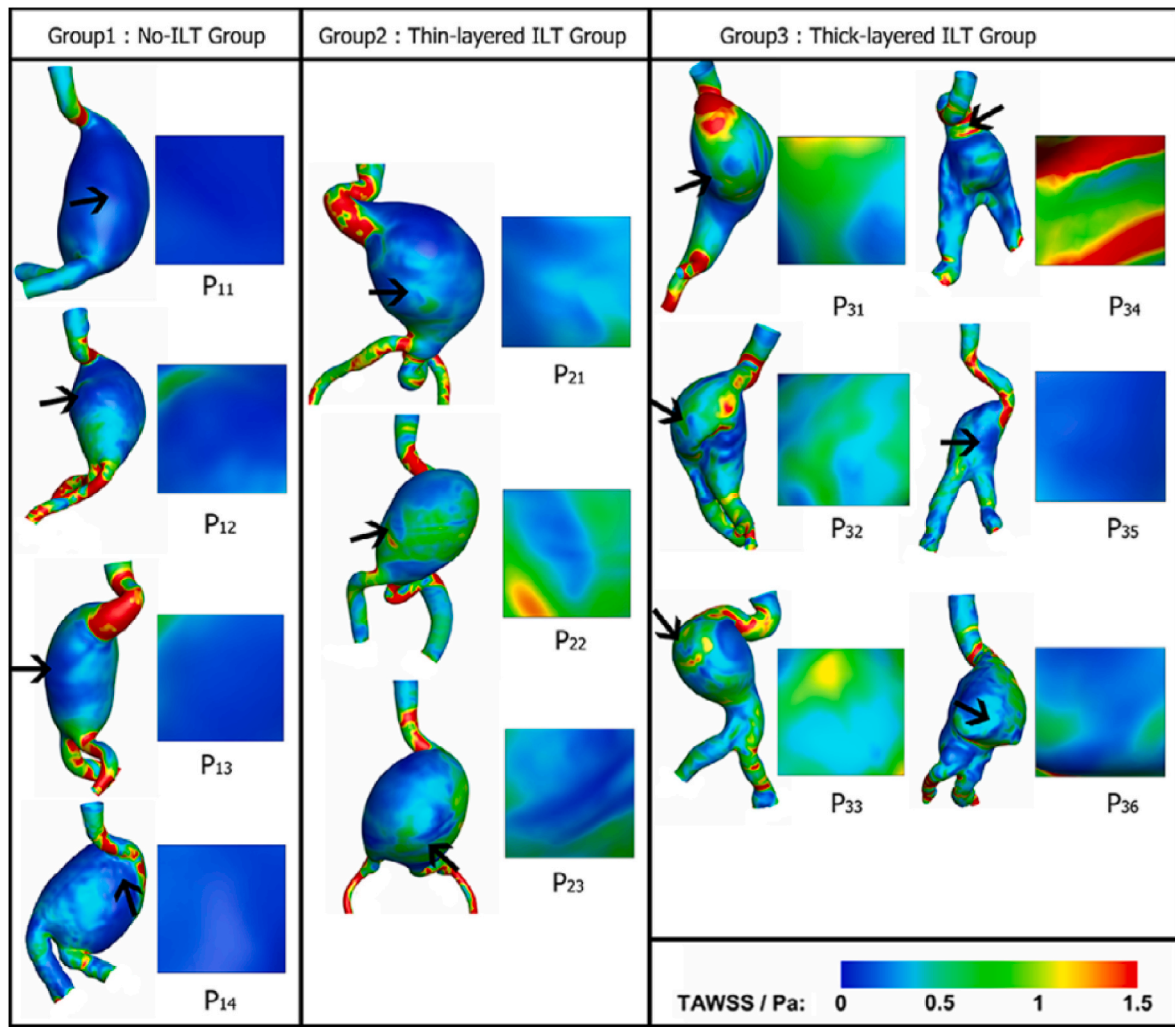
Fig. 3. TAWSS contour maps of different patients ruptured (indicated with black arrows) AAA with and without ILT deposition. The figure is adapted from Ref. [54] and used with permission.

Table 2
Summarized data for 100-time steps considering a sample case which is composed of 2000 elements on the AAA wall.

Time step = 1	WSSx	WSSy	WSSz
Element number = 1	0.61	0.42	0.12
Element number = 2	0.60	0.46	0.21
…	…	…	…
Element number = 2000	0.10	0.30	0.23
…	…	…	…
Time step = 100	**WSSx**	**WSSy**	**WSSz**
Element number = 1	0.11	0.08	0.02
Element number = 2	0.20	0.10	0.08
…	…	…	…
Element number = 2000	0.12	0.05	0.01

Table 3
Calculated WSS magnitudes at each time step.

Time step = 1	$|\tau_w|$
Element number = 1	0.750
Element number = 2	0.784
…	…
Element number = 2000	0.391
…	…
Time step = 100	$|\tau_w|$
Element number = 1	0.137
Element number = 2	0.237
…	…
Element number = 2000	0.130

element (for 2000 elements in the sample case) on the AAA wall as shown in Table 4.

$$\text{TAWSS}_n = \frac{1}{T}\left(\int_0^T |\tau_w| dt\right) \approx \frac{1}{T}\left(\sum_{k=1}^{T_k} \Delta t |\tau_w|_n\right) = \frac{\Delta t}{T}\left(\sum_{k=1}^{100} |\tau_w|_n\right)$$
$$= \frac{1}{100}\left(|\tau_w|_{n,Total}\right) \tag{8}$$

3.2. OSI (Oscillatory shear index)

OSI is another critical hemodynamic parameter that explains the periodic separation of WSS from the prevailing axial direction. In Fig. 4, OSI values are provided for ten different patient-specific AAAs, and a highly heterogenous OSI map is obtained on the AAA wall of each sample case. Ku et al. proposed the original concept of OSI [85], but since the definition lacks a dominant axial direction, the equation cannot be extended to a general three-dimensional form. As a result, He et al. proposed an alternative definition of OSI, as shown in Eq. (9),

Table 4
TAWSS calculation for each mesh point.

	Tstep = 1	$|\tau_w|$		Tstep = 2	$|\tau_w|$				Tstep = 100	$|\tau_w|$
$|\tau_w|_{Total} =$	E. 1	0.750		E. 1	0.530				E. 1	0.137
	E. 2	0.784	+	E. 2	0.644	+	...	+	E. 2	0.237
	...	...		...	...				...	...
	E. 2000	0.391		E. 2000	0.312				E. 2000	0.130
										TAWSS
Element number = 1										0.70
Element number = 2										0.79
...										...
Element number = 2000										0.43
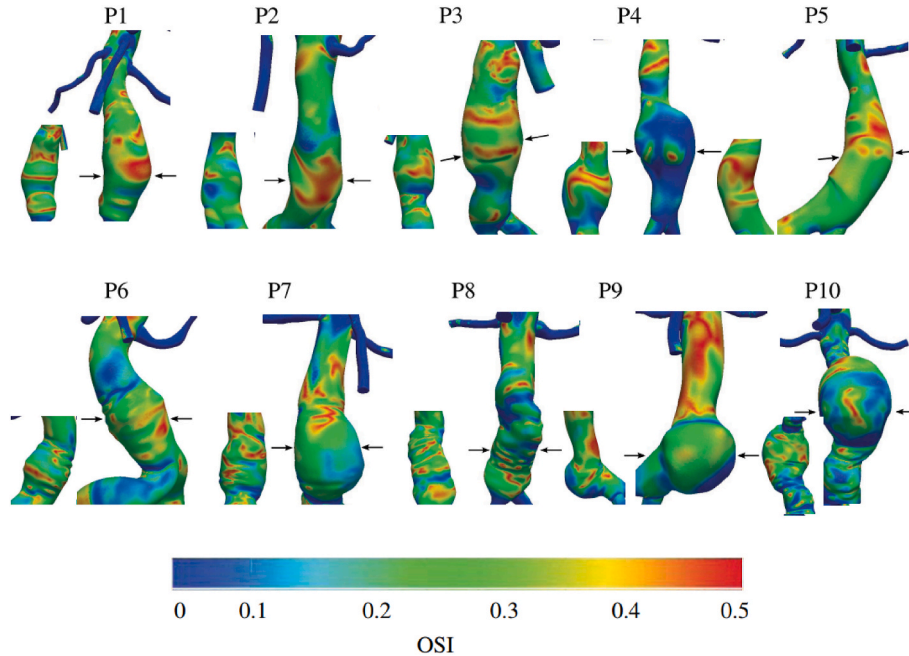
Fig. 4. OSI results for the ten different patient hemodynamic CFD simulations. The figure is adapted from Ref. [57] and used with permission.

which is now widely used and approved by many researchers [86]. As shown in Eq. (9), OSI can be written in various forms.

$$OSI = \frac{1}{2}\left(1 - \frac{\left|\int_0^T \tau_w \, dt\right|}{\int_0^T |\tau_w| \, dt}\right) = \frac{1}{2}\left(1 - \frac{\frac{1}{T}\left|\int_0^T \tau_w \, dt\right|}{\frac{1}{T}\int_0^T |\tau_w| \, dt}\right) = \frac{1}{2}\left(1 - \frac{\frac{1}{T}\left|\int_0^T \tau_w \, dt\right|}{TAWSS}\right)$$

(9)

OSI values range from 0 to 0.5, with 0 indicating a fully unidirectional WSS and 0.5 indicating WSS with a temporal average of zero [78, 80,87]. For all the presented forms in Eq. (9), OSI is obtained by dividing

the WSS vector by the WSS magnitude.

For calculating OSI in a CFD simulation, total WSS vectors should be determined at each mesh point considering Eq. (10), where $\tau_{wn,total}$ denotes the summation of all WSS vectors at the element number n within one full cardiac cycle. Due to summing up the WSS vectors, three spatial components of WSS in x, y, and z directions should be summed separately, as shown in Table 5.

$$T_{wn,total} = \int_0^T \tau_w \, dt$$

(10)

After determining the summation of WSS vector components in x, y, and z directions, the total magnitude of WSS can be found using the

Table 5
Calculation of total WSS vector magnitudes for each mesh element.

	Tstep = 1	WSSx	WSSy	WSSsz		Tstep = 2	WSSx	WSSy	WSSz			Tstep = 100	WSSx	WSSy	WSSz
$\tau_{w\,total} =$	E.1	0.61	0.42	0.12		E.1	0.56	0.38	0.11			E.1	0.11	0.08	0.02
	E.2	0.60	0.46	0.21	+	E.2	0.57	0.54	0.28	+	... +	E.2	0.20	0.10	0.08
	...	...	...	...		...	...	...	...			...	...	...	...
	E.2000	0.10	0.30	0.23		E.2000	0.11	0.33	0.17			E.2000	0.12	0.05	0.01
							WSSx total			WSSy total			WSSz total		
$\tau_{w\,total} =$			Element number = 1				53			33			10		
			Element number = 2				49			51			15		
			...				...			...			...		
			Element number = 2000				25			19			17		

Pythagorean theorem, which is previously given in Eq. (6). For the given sample case with 2000 elements, the magnitudes of total WSS vectors are provided in Table 6.

Finally, the TAWSS values provided in Table 4 and the total magnitudes of the WSS vectors ($|\tau_{wtotal}|$) given in Table 6 can be used to determine the values of OSI. In Eq. (11), the value of OSI is determined for the 1st element of the given sample case. Using the same procedure, the OSI values can be determined for each mesh element of the sample case, as shown in Table 7.

$$\text{OSI}_{for\ element\ 1} = \frac{1}{2}\left(1 - \frac{\frac{1}{100}(63.23)}{0.70}\right) = 0.048 \tag{11}$$

3.3. ECAP (Endothelial cell activation potential)

The ECAP metric is proposed by Di Achile et al. and employs the ratio of OSI and TAWSS to describe the vessel wall's thrombogenic susceptibility, as provided in Eq. (12) [88]. ECAP is used to identify the areas which are exposed to high OSI and low TAWSS as shown in Fig. 5. High ECAP index values will correspond to the conditions of large OSI and small TAWSS, which is indicating endothelial sensitivity [88].

$$ECAP = \frac{OSI}{TAWSS} \tag{12}$$

3.4. RRT (Relative residence time)

According to Himburg et al. [89], the combination of TAWSS and OSI reflects the time that blood spends near the vessel wall. This resulted in the creation of a new metric called RRT, which is used to assess the state of the degraded flow as shown in Fig. 6 [89]. Since RRT is the inverse of the time-averaged WSS vector magnitude, it has a near-perfect correlation with TAWSS. Consequently, it's been proposed that RRT might take the place of WSS and OSI as a single descriptor of "low and oscillating" shear stress [90]. The definition of the RRT is given in Eq. (13). It should be noted that RRT is inversely proportional to the numerator of OSI, as shown in Eq. (14).

$$RRT = \frac{1}{(1 - 2 \times OSI) \times TAWSS} \tag{13}$$

$$RRT = \frac{1}{\frac{1}{T}\left|\int_0^T \tau_w\ dt\right|} \tag{14}$$

4. Recent studies on WSS (Wall shear stress) related hemodynamic parameters and rupture risk assessment

Different techniques are being developed by clinicians to precisely predict the likelihood of aneurysm rupture. However, rather than being founded on solid physical principles, practically all of the criteria that have been developed are based on empirical data. "Laplace's law" is the criterion that is most usually utilized [92]. According to Laplace's law, which serves as the theoretical basis for the maximum diameter criterion, the mechanical stress acting on the aneurysm wall is directly proportional to its diameter. In most cases, AAA geometries do not have a specified simple spherical structure. On the contrary, it is unique to each patient and geometrically complex [93,94]. The geometric

Table 6
Total WSS vector magnitudes at each mesh element within one cardiac cycle.

		$|T_{wtotal}|$
$|\tau_{wtotal}| =$	Element number = 1	63.23
	Element number = 2	72.30
	…	…
	Element number = 2000	35.70

Table 7
OSI calculation for each mesh element.

	OSI
Element number = 1	0.048
Element number = 2	0.042
…	…
Element number = 2000	0.084

structure of the aneurysm sac as well as the diameter and degree of curvature of the artery exiting the aneurysm have a direct impact on the blood flow dynamics in the AAA sac and the associated shear stresses acting on the wall. Therefore, only measuring the maximum diameter using the standard imaging methods may be insufficient to correctly assess the risk of rupture potential [95,96], because the factors such as AAA expansion rate [97–99], wall stiffness, increased ILT thickness [100], wall tension [17], and peak AAA wall stress [36,37,44] have been suggested as additional potential predictors of AAA rupture [14].

While biomechanical assessment of degenerated AAA is important in assessing the rupture risk, mechanical stresses on the tissue cannot be directly extracted from the clinical images. Mechanical wall stress and WSS can be calculated by performing computational analysis based on finite element formulations. For this purpose, CFD simulations are performed using realistic boundary conditions. The steady flow analysis is not appropriate for modeling the pulsatile nature of the blood flow. Therefore, time-dependent transient CFD analysis with time-varying inlet and outlet boundary conditions should be applied for an accurate flow simulation.

Evaluation of WSS magnitudes at specific time points such as at the instant of peak flow velocity is ineffective in determining the critical locations on the aneurysm sac because of the collective hemodynamic effects taking place during the entire cardiac cycle that regulates the aneurysm expansion or rupture. Therefore, examining the average of the forces exerted on the wall during the entire cardiac cycle is critical for determining the suspected zones of rupture. It should be noted that analyzing TAWSS alone is generally insufficient to detect the significant locations with a high risk of rupture. Therefore, using multiple parameters such as OSI, ECAP, and RRT in combination with TAWSS would increase the reliability of the rupture risk assessment and result in more effective predictive outcomes.

4.1. Effects of WSS (Wall shear stress) and TAWSS (Time average wall shear stress)

Recent studies have shown that low WSS on the vessel wall is a risk factor and it is associated with the formation of atherosclerosis and aneurysm growth [87,101]. Long-term exposure to low WSS on the aneurysm wall increases intercellular permeability [102] and induces severe elasticity degradation in the aneurysm sac [103]. In addition, oscillatory and irregular WSS levels below 0.4 Pa increase the development of atherosclerosis by resulting in endothelial cell degeneration [22,79,104]. The physiological WSS values are determined to be between 1 and 5 Pa in large arteries [105]. When endothelial cells are subjected to WSS levels in the stated physiological range, their anti-inflammatory and anti-thrombogenic responses change, and the vascular remodeling mechanism initiates. Therefore, WSS levels within the physiological limitations have a positive effect on vascular health [106–108]. The low WSS environment may facilitate conditions that favor the activation of coagulation factors which promote platelet adhesion and the subsequent plate deposition in addition to the proliferation of ILT in the flow recirculation zones [34,53,109–112].

Although TAWSS is a significant component in modulating ILT deposition, there is no increase in the ILT thickness in the regions with low TAWSS. This fact indicates that another flow feature such as vortex dynamics may be controlling the amount of thrombus that can form across the luminal wall [113]. The decrease in TAWSS level which is
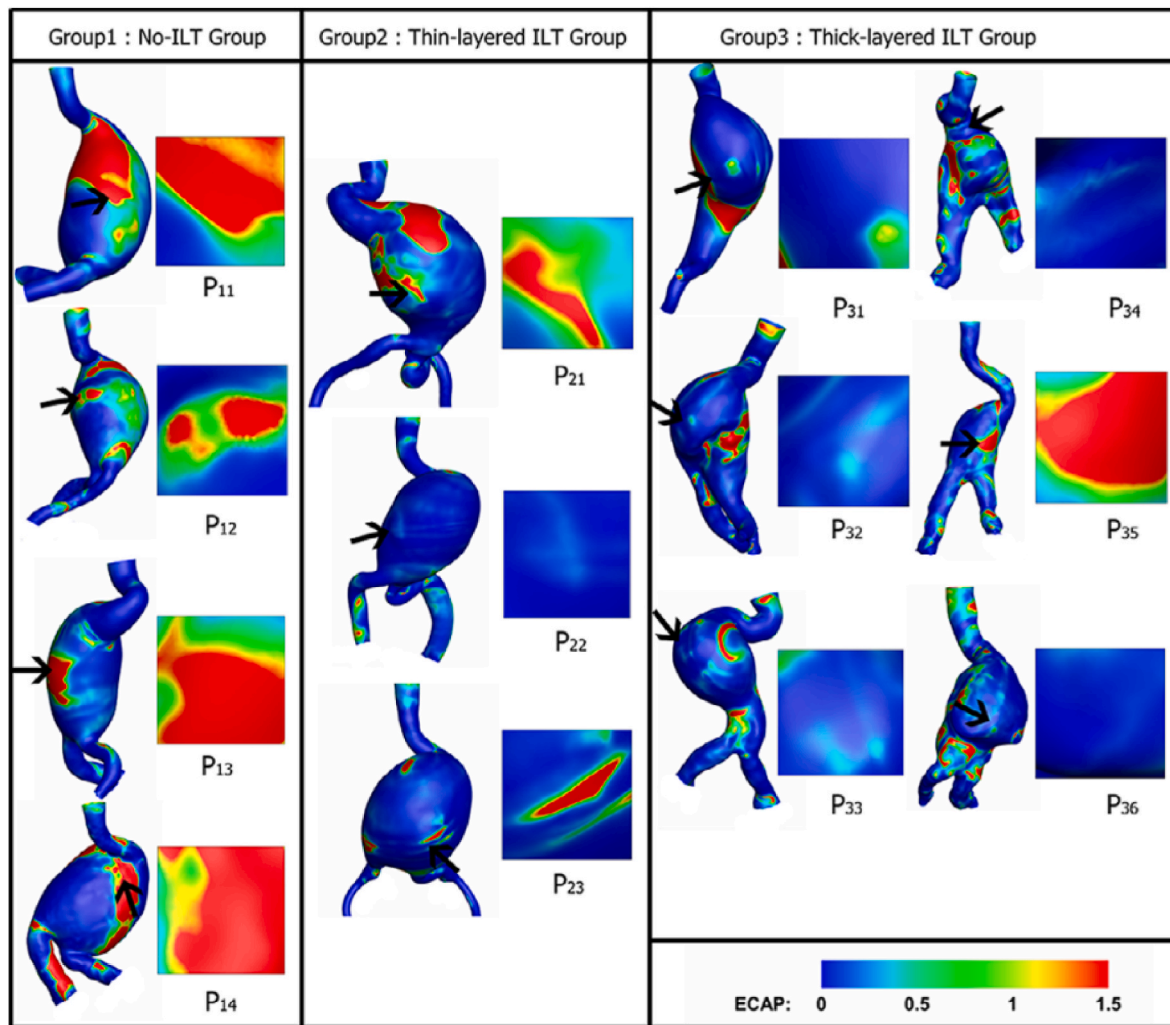
Fig. 5. ECAP contour maps of different patient hemodynamic CFD simulations ruptured (indicated with black arrows) AAA with and without ILT deposition. The figure is adapted from Ref. [54] and used with permission.

caused by the slow circulation observed in the AAA sac causes an enlargement of the AAA [38]. In addition, it is observed that AAA growth rate [114] and rupture [51,52] are associated with low TAWSS and high ILT accumulation.

According to several studies, aneurysm rupture in the regions of low WSS [53] has been associated with the accumulation of ILT in these regions [54,55] and the occurrence of aortic wall hypoxia [115,116], which causes local wall disruption that is more sensitive to rupture. On the contrary, another study demonstrates that the high WSS levels (WSS >3 Pa [117]) on the AAA wall are related to the aneurysm rupture [34, 118].

4.2. Effects of OSI (Oscillatory shear index) and ECAP (Endothelial cell activation potential)

The phenotypic regulation of AAA development is observed to be correlated with high blood pressure, increased medial thickness, and high OSI, which are all correlated with cell inflammation [118,119]. OSI, on the other hand, is related to thrombus formation and growth, indicating that OSI and ILT correlate [120]. It is observed that there is significant thrombus growth in regions with low OSI (<0.1) values. In contrast to thrombus formation, there is limited or no thrombus growth when the TAWSS level is low and OSI exceeds 0.1 [56,121]. Lozowy et al. reported no direct link between OSI and ILT deposition in 23 AAA cases with a diameter greater than 5 cm, which was caused by abnormal

flows in large-diameter AAA, in contrast to typical flows in small-diameter AAAs [122]. However, Zambrano et al. showed in their study that the accumulation of ILT occurs in both high and low OSI values [113].

The examination of TAWSS and OSI combined is important for detecting critical regions on the vessel or aneurysm wall. Previous studies have shown that the combination of low TAWSS and high OSI may result in intravascular abnormalities which are also related to aneurysm growth and rupture [56,70,114,120,123]. Arzani et al. discovered that thrombus growth is common in the areas with TAWSS between 2 and 3 dyn/cm^2, and there is a significant negative relationship between OSI and thrombus accumulation. However, ILT accumulation is not observed in regions with high OSI (>0.4) and low TAWSS values (<0.1 Pa) [57].

4.3. Effects of ILT (Intraluminal thrombus deposition), RRT (Relative Residence time), and ECAP (Endothelial cell activation potential)

TAWSS, OSI, and ECAP (shown in Fig. 7) were shown to be good predictors to obtain critical rupture locations when ruptured or non-ruptured AAA surfaces were examined. In some cases, however, determining the rupture location by using a fixed TAWSS, OSI, or ECAP threshold value is not practical. The accumulation of ILT, which occurs as a result of hemodynamic factors, affects the WSS on the aneurysm sac as well as the mechanical properties of the wall such as wall elasticity
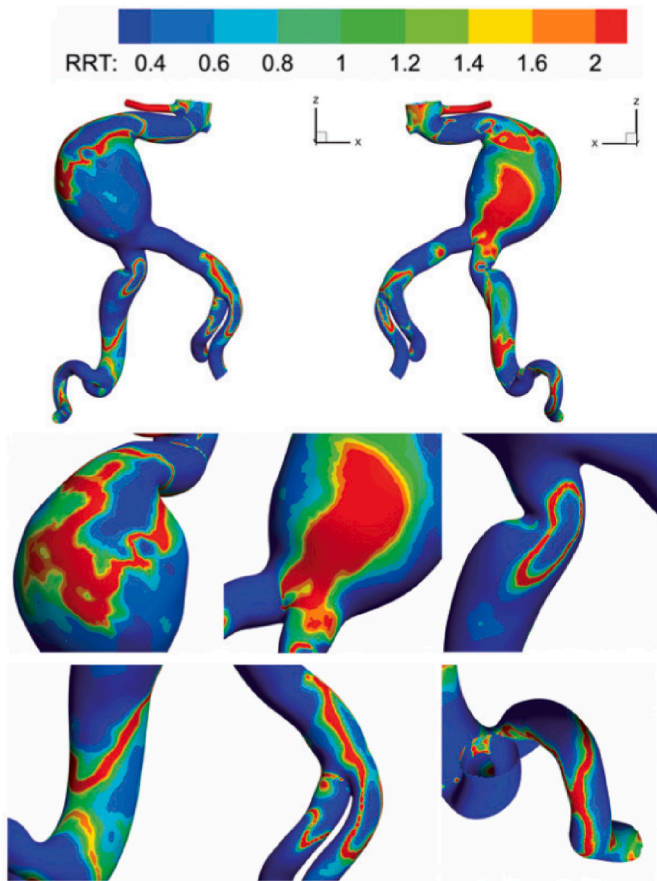
Fig. 6. RRT contour map of an AAA. The figure is adapted from Ref. [91] and used with permission.

and thickness. Since these factors affect the rupture of the degenerative wall as well, the presence and level of ILT on the aneurysmal wall should also be taken into consideration.

A recent study compared three different groups of ruptured AAA: AAA without ILT, AAA with thin-layer ILT, and AAA with thick-layer ILT deposition. For the AAAs without ILT, the rupture was detected in regions with low TAWSS, high OSI, and high ECAP. On the other hand, for the AAAs with thick-layered ILT, rupture is observed at regions with high TAWSS and low ECAP. Interestingly, for the AAAs with medium ILT thickness, there was no direct correlation between the risk of rupture and TAWSS, OSI, or ECAP [54].

According to the studies investigating RRT and ECAP, the long residence time associated with recirculation areas is considered to provide the exposure time required for activated platelets to adhere to the thrombogenic/atherogenic surface [77,101]. RRT demonstrated a continuous positive correlation with thrombus growth [120]. ECAP values close to 1.4 Pa^{-1} and higher are used by Kelsey et al. to identify the critical thrombus locations. Furthermore, it was found that the locations with the highest ECAP and the longest residence duration were more prone to thrombus development [124].

5. Conclusion and future directions

Disturbed hemodynamics has been known to influence the progression of AAAs. Several parameters have been proposed to characterize disturbed hemodynamics for cardiovascular flows. Among these, TAWSS, OSI, ECAP, and RRT are the ones most applied to AAA investigations. There seems to be some confusion regarding the calculation of these parameters, which is not straightforward. Here, we explain these WSS-derived parameters focusing on how they represent different characteristics of disturbed hemodynamics. A representative case was presented for spatial and temporal formulation that would be useful for interested researchers for practical calculations. We also summarized recent findings, relating WSS-related parameters with AAA rupture risk assessment.

As well-known WSS-related parameters, TAWSS and OSI are associated with endothelial sensing-mediated vascular remodeling [125, 126]. ECAP [88] is the ratio of OSI and TAWSS, characterizing the thrombogenic susceptibility on the arterial wall. RRT has been recently developed as a new hemodynamic component to describe the relatively slower flow characteristics near the aneurysm wall [23,90].

In many studies, it is reported that the low WSS environment in AAA sac results in wall tissue degradation and ILT accumulation, which deteriorates the mechanical strength of the arterial wall and increases the risk of rupture. There are also investigations showing that high WSS affects the increased rupture risk. In the small diameter AAAs, low OSI levels promote the ILT formation in the aneurysm sac. However, when
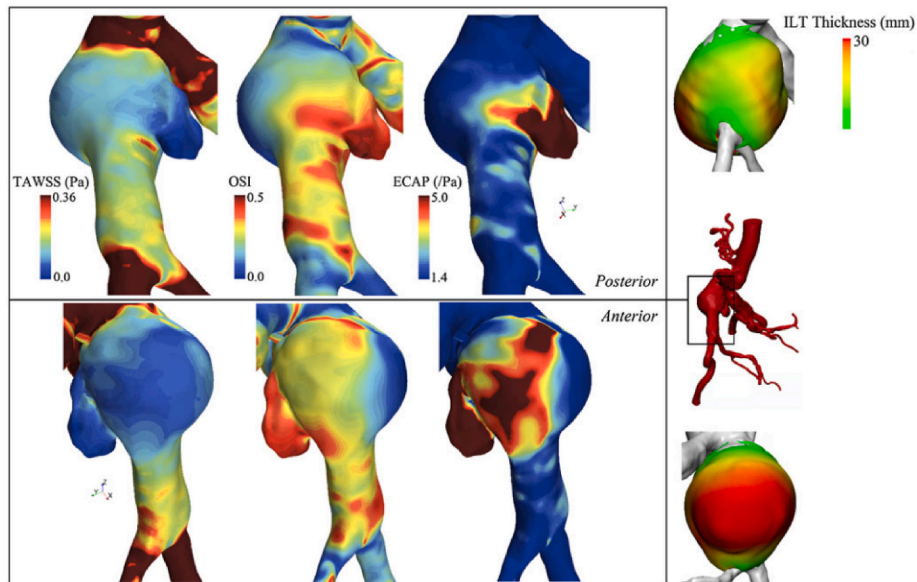
Fig. 7. TAWSS, OSI, and ECAP fields for a saccular AAA case. The figure is adapted from Ref. [124] and used with permission.

the AAA diameter is increased, OSI values are not effective on the ILT deposit. The general opinion is that the low TAWSS combined with high OSI leads to abnormal conditions which may result in AAA enlargement or rupture. Interestingly, the presence of ILT introduces many uncertainties in the problem, and the conclusions mentioned above are no longer valid depending on the thickness and shape of the ILT.

In conclusion, WSS-related parameters are very important for characterizing cardiovascular flows and they show great promise for the assessment of disease severity as in the case of AAAs for predicting rupture risk. While most studied parameters are TAWSS, OSI, ECAP, and RRT, newer parameters are constantly being introduced such as wall shear stress exposure time (WSSET) and time-averaged WSS divergence (WSSdiv) [57,75,127] to better represent the disturbed hemodynamics in cardiovascular flows. Advancing CFD tools and approaches are expected to result in more practical and faster CFD runs and better use of WSS-derived parameters in clinical cardiovascular practice.

Declaration of competing interest

The authors declare that there is no conflict of interest.

Acknowledgments

References

[1] E. Bossone, K.A. Eagle, Epidemiology and management of aortic disease: aortic aneurysms and acute aortic syndromes, Nat. Rev. Cardiol. 18 (5) (May 2021) 331–348, https://doi.org/10.1038/S41569-020-00472-6.

[2] U.K.A. Sampson, et al., Global and regional burden of aortic dissection and aneurysms: mortality trends in 21 world regions, 1990 to 2010, Glob. Heart 9 (1) (2014) 171–180.e10, https://doi.org/10.1016/J.GHEART.2013.12.010.

[3] T.M. McGloughlin, B.J. Doyle, New approaches to abdominal aortic aneurysm rupture risk assessment: engineering insights with clinical gain, Arterioscler. Thromb. Vasc. Biol. 30 (9) (2010) 1687–1694, https://doi.org/10.1161/ATVBAHA.110.204529.

[4] N. Sakalihasan, R. Limet, O. Defawe, Abdominal aortic aneurysm, Lancet 365 (9470) (2005) 1577–1589, https://doi.org/10.1016/S0140-6736(05)66459-8.

[5] N. Kontopodis, E. Metaxa, Y. Papaharilaou, E. Tavlas, D. Tsetis, C. Ioannou, Advancements in identifying biomechanical determinants for abdominal aortic aneurysm rupture, Vascular 23 (1) (2015) 65–77, https://doi.org/10.1177/1708538114532084.

[6] A. Anjum, R. von Allmen, R. Greenhalgh, Explaining the decrease in mortality from abdominal aortic aneurysm rupture, J. Vasc. Surg. 56 (3) (2012) 876, https://doi.org/10.1016/j.jvs.2012.07.017.

[7] T.B.M. Wilmink, C.R.G. Quick, C.S. Hubbard, N.E. Day, The influence of screening on the incidence of ruptured abdominal aortic aneurysms, J. Vasc. Surg. 30 (2) (1999) 203–208, https://doi.org/10.1016/S0741-5214(99)70129-1.

[8] H. Bengtsson, D. Bergqvist, Ruptured abdominal aortic aneurysm: a population-based study, J. Vasc. Surg. 18 (1) (1993) 74–80, https://doi.org/10.1067/mva.1993.42107.

[9] M.P. Nevitt, D.J. Ballard, J.W.J. Hallett, Prognosis of abdominal aortic aneurysms, N. Engl. J. Med. 25 (3) (2010) 167–176, https://doi.org/10.1056/NEJM198910123211504. Jan.

[10] J. Jin, Screening for abdominal aortic aneurysm, JAMA, J. Am. Med. Assoc. 322 (22) (2019) 2256, https://doi.org/10.1001/jama.2019.19338.

[11] M.T. Menard, et al., Thoracoviscteral segment aneurysm repair after previous infrarenal abdominal aortic aneurysm surgery, J. Vasc. Surg. 39 (6) (2004) 1163–1170, https://doi.org/10.1016/J.JVS.2003.12.019.

[12] R.C. Darling, C.R. Messina, D.C. Brewster, L.W. Ottinger, Autopsy study of unoperated abdominal aortic aneurysms. The case for early resection, Circulation 56 (suppl. 2) (1977) 161–164, 3.

[13] F.L. Moll, et al., Management of abdominal aortic aneurysms clinical practice guidelines of the European society for vascular surgery, Eur. J. Vasc. Endovasc. Surg. 41 (SUPPL. 1) (2011), https://doi.org/10.1016/j.ejvs.2010.09.011.

[14] D.A. Vorp, Biomechanics of abdominal aortic aneurysm, J. Biomech. 40 (9) (2007) 1887–1902, https://doi.org/10.1016/j.jbiomech.2006.09.003. Jan.

[15] S.C. Nicholls, J.B. Gardner, M.H. Meissner, K.H. Johansen, Rupture in small abdominal aortic aneurysms, J. Vasc. Surg. 28 (5) (Nov. 1998) 884–888, https://doi.org/10.1016/S0741-5214(98)70065-5.

[16] S.A. Choksy, A.B.M. Wilmink, C.R. Quick, Ruptured abdominal aortic aneurysm in the Huntingdon district: a 10-year experience, Ann. R. Coll. Surg. Engl. 81 (1) (Jan. 1999) 27. Accessed: Jul. 27, 2022. [Online]. Available:.

[17] A.J. Hall, E.F.G. Busse, D.J. McCarville, J.J. Burgess, Aortic wall tension as a predictive factor for abdominal aortic aneurysm rupture: improving the selection of patients for abdominal aortic aneurysm repair, 2000 142, Ann. Vasc. Surg. 14 (2) (2014) 152–157, https://doi.org/10.1007/S100169910027. Feb.

[18] P. Jt, et al., Long-term outcomes of immediate repair compared with surveillance of small abdominal aortic aneurysms, N. Engl. J. Med. 346 (19) (May 2002) 1445–1452, https://doi.org/10.1056/NEJMOA013527.

[19] H.E. Salman, B. Ramazanli, M.M. Yavuz, H.C. Yalcin, Biomechanical investigation of disturbed hemodynamics-induced tissue degeneration in abdominal aortic aneurysms using computational and experimental techniques, Front. Bioeng. Biotechnol. 7 (111) (May 2019) 111, https://doi.org/10.3389/fbioe.2019.00111.

[20] H.E. Salman, et al., Effect of left atrial ligation-driven altered inflow hemodynamics on embryonic heart development: clues for prenatal progression of hypoplastic left heart syndrome, Biomech. Model. Mechanobiol. 20 (2) (Apr. 2021) 733–750, https://doi.org/10.1007/S10237-020-01413-5/FIGURES/16.

[21] H.E. Salman, H.C. Yalcin, Computational investigation of the effect of wall thickness on rupture risk in abdominal aortic aneurysms, J. Appl. Fluid Mech. 14 (2) (2021) 499–513, https://doi.org/10.47176/jafm.14.02.31727.

[22] A.M. Malek, Hemodynamic shear stress and its role in atherosclerosis, JAMA 282 (21) (1999) 2035, https://doi.org/10.1001/jama.282.21.2035. Dec.

[23] J. Xiang, et al., Hemodynamic-morphologic discriminants for intracranial aneurysm rupture, Stroke 42 (1) (2011) 144–152, https://doi.org/10.1161/STROKEAHA.110.592923.

[24] A. Roldán-Alzate, C.J. Francois, O. Wieben, S.B. Reeder, Emerging applications of abdominal 4D flow MRI, Am. J. Roentgenol. 207 (1) (2016) 58–66, https://doi.org/10.2214/AJR.15.15995.

[25] A. Feintuch, et al., Hemodynamics in the mouse aortic arch as assessed by MRI, ultrasound, and numerical modeling, Am. J. Physiol. Heart Circ. Physiol. 292 (2) (2007) 884–892, https://doi.org/10.1152/ajpheart.00796.2006.

[26] Z. Stankovic et al., "A Feasibility Study to Evaluate Splanchnic Arterial and Venous Hemodynamics by Flow-Sensitive 4D MRI Compared with Doppler Ultrasound in Patients with Cirrhosis and Controls," pp. 669–675, doi: 10.1097/MEG.0b013e32835e1297.

[27] A. Harloff, et al., 3D Blood Flow Characteristics in the Carotid Artery Bifurcation Assessed by Flow-Sensitive 4D MRI at 3T, vol. 74, 2009, pp. 65–74, https://doi.org/10.1002/mrm.21774. June 2008.

[28] S. Mahinrad, et al., Intracranial blood flow quantification by accelerated dual-venc 4D flow MRI: comparison with transcranial Doppler ultrasound, J. Magn. Reson. Imag. (2022) 1–9, https://doi.org/10.1002/jmri.28115.

[29] F.M. Benslimane, M. Alser, Z.Z. Zakaria, A. Sharma, H.A. Abdelrahman, H. C. Yalcin, Adaptation of a mice Doppler echocardiography platform to measure cardiac flow velocities for embryonic chicken and adult zebrafish, Front. Bioeng. Biotechnol. 7 (May 2019) 96, https://doi.org/10.3389/FBIOE.2019.00096.

[30] A. Azarine, et al., Four-dimensional flow MRI: principles and cardiovascular applications, Radiographics 39 (3) (May 2019) 632–648, https://doi.org/10.1148/RG.2019180091/ASSET/IMAGES/LARGE/RG.2019180091.FIG16C.JPEG.

[31] A.B.B. Olcay, A. Amindari, K. Kirkkopru, H.C.C. Yalcin, Characterization of disturbed hemodynamics due to stenosed aortic jets with a Lagrangian Coherent structures technique, J. Appl. Fluid Mech. 11 (2) (2018) 1735–3645, https://doi.org/10.18869/acadpub.jafm.73.245.28185.

[32] H.E. Salman, L. Saltik, H.C. Yalcin, Computational analysis of wall shear stress patterns on calcified and bicuspid aortic valves: focus on radial and coaptation patterns, Fluids 6 (2021) 8, https://doi.org/10.3390/FLUIDS6080287.

[33] O. Mutlu, H.E. Salman, H.C. Yalcin, A.B. Olcay, Fluid flow characteristics of healthy and calcified aortic valves using three-dimensional Lagrangian coherent structures analysis, Fluids 6 (2021) 6, https://doi.org/10.3390/FLUIDS6060203.

[34] M. Xenos, et al., Patient-based abdominal aortic aneurysm rupture risk prediction with fluid structure interaction modeling, Ann. Biomed. Eng. 38 (11) (2010) 3323–3337, https://doi.org/10.1007/s10439-010-0094-3.

[35] Y. Qiu, D. Yuan, J. Wen, Y. Fan, T. Zheng, Numerical identification of the rupture locations in patient-specific abdominal aortic aneurysmsusing hemodynamic parameters, Comput. Methods Biomech. Biomed. Eng. 21 (1) (2018) 1–12, https://doi.org/10.1080/10255842.2017.1410796.

[36] M.F. Fillinger, M.L. Raghavan, S.P. Marra, J.L. Cronenwett, F.E. Kennedy, In vivo analysis of mechanical wall stress and abdominal aortic aneurysm rupture risk, J. Vasc. Surg. 36 (3) (2002) 589–597, https://doi.org/10.1067/MVA.2002.125478.

[37] A.K. Venkatasubramaniam, et al., A comparative study of aortic wall stress using finite element analysis for ruptured and non-ruptured abdominal aortic aneurysms, Eur. J. Vasc. Endovasc. Surg. 28 (2) (Aug. 2004) 168–176, https://doi.org/10.1016/J.EJVS.2004.03.029.

[38] X. Wang, X. Li, A fluid-structure interaction-based numerical investigation on the evolution of stress, strength and rupture potential of an abdominal aortic aneurysm, Comput. Methods Biomech. Biomed. Eng. 16 (9) (2013) 1032–1039, https://doi.org/10.1080/10255842.2011.652097.

[39] T. Canchi, S.D. Kumar, E.Y.K. Ng, S. Narayanan, A review of computational methods to predict the risk of rupture of abdominal aortic aneurysms, BioMed Res. Int. 2015 (2015), https://doi.org/10.1155/2015/861627.

[40] S.N. Lipp, et al., Computational hemodynamic modeling of arterial aneurysms: a mini-review, Front. Physiol. 11 (May 2020) 454, https://doi.org/10.3389/FPHYS.2020.00454/BIBTEX.

[41] S. Polzer, T.C. Gasser, Biomechanical rupture risk assessment of abdominal aortic aneurysms based on a novel probabilistic rupture risk index, J. R. Soc. Interface 12 (2015) 113, https://doi.org/10.1098/RSIF.2015.0852. Dec.

[42] M.F. Fillinger, The long-term relationship of wall stress to the natural history of abdominal aortic aneurysms (finite element analysis and other methods), Ann. N. Y. Acad. Sci. 1085 (2006) 22–28, https://doi.org/10.1196/ANNALS.1383.037.

[43] P. Rissland, Y. Alemu, S. Einav, J. Ricotta, D. Bluestein, Abdominal aortic aneurysm risk of rupture: patient-specific FSI simulations using anisotropic model, J. Biomech. Eng. 131 (3) (2009) 1–10, https://doi.org/10.1115/1.3005200.

[44] M.F. Fillinger, S.P. Marra, M.L. Raghavan, F.E. Kennedy, Prediction of rupture risk in abdominal aortic aneurysm during observation: wall stress versus diameter, J. Vasc. Surg. 37 (4) (Apr. 2003) 724–732, https://doi.org/10.1067/MVA.2003.213.

[45] M. Truijers, J.A. Pol, L.J. SchultzeKool, S.M. van Sterkenburg, M.F. Fillinger, J. D. Blankensteijn, Wall stress analysis in small asymptomatic, symptomatic and ruptured abdominal aortic aneurysms, Eur. J. Vasc. Endovasc. Surg. 33 (4) (Apr. 2007) 401–407, https://doi.org/10.1016/J.EJVS.2006.10.009.

[46] C.M. Scotti, A.D. Shkolnik, S.C. Muluk, E.A. Finol, Fluid-structure interaction in abdominal aortic aneurysms: effects of asymmetry and wall thickness, Biomed. Eng. Online 4 (–22) (2005) 1, https://doi.org/10.1186/1475-925X-4-64.

[47] E.S. Di Martino, D.A. Vorp, Effect of variation in intraluminal thrombus constitutive properties on abdominal aortic aneurysm wall stress, Ann. Biomed. Eng. 31 (7) (2003) 804–809, https://doi.org/10.1114/1.1581880.

[48] E. Di Martino, et al., Biomechanics of abdominal aortic aneurysm in the presence of endoluminal thrombus: experimental characterisation and structural static computational analysis, Eur. J. Vasc. Endovasc. Surg. 15 (4) (1998) 290–299, https://doi.org/10.1016/S1078-5884(98)80031-2.

[49] E.S. Di Martino, et al., Fluid–structure interaction within realistic three-dimensional models of the aneurysmatic aorta as a guidance to assess the risk of rupture of the aneurysm, Med. Eng. Phys. 23 (9) (2001) 647–655, https://doi.org/10.1016/S1350-4533(01)00093-5.

[50] E.S. Di Martino, A. Bohra, J.P. Vande Geest, N. Gupta, M.S. Makaroun, D.A. Vorp, Biomechanical properties of ruptured versus electively repaired abdominal aortic aneurysm wall tissue, J. Vasc. Surg. 43 (3) (Mar. 2006) 570–576, https://doi.org/10.1016/J.JVS.2005.10.012.

[51] A. Forneris, F.B. Marotti, A. Satriano, R.D. Moore, E.S. Di Martino, A novel combined fluid dynamic and strain analysis approach identified abdominal aortic aneurysm rupture, J. Vasc. Surg. Cases Innov. Tech. 6 (2) (2020) 172–176, https://doi.org/10.1016/j.jvscit.2020.01.014.

[52] B.J. Doyle, T.M. McGloughlin, E.G. Kavanagh, P.R. Hoskins, From detection to rupture: a serial computational fluid dynamics case study of a rapidly expanding, patient-specific, ruptured abdominal aortic aneurysm, Comput. Biomech. Med. Fundam. Sci. Patient-Specific Appl. 9781493907 (2014) 53–68, https://doi.org/10.1007/978-1-4939-0745-8_5/FIGURES/8. Feb.

[53] D.B. McClarty, D.C.S. Kuhn, A.J. Boyd, Hemodynamic changes in an actively rupturing abdominal aortic aneurysm, J. Vasc. Res. 58 (3) (2021) 172–179, https://doi.org/10.1159/000514237.

[54] Y. Qiu, et al., Role of intraluminal thrombus in abdominal aortic aneurysm ruptures: a hemodynamic point of view, Med. Phys. 46 (9) (2019) 4263–4275, https://doi.org/10.1002/mp.13658.

[55] A.J. Boyd, D.C.S. Kuhn, R.J. Lozowy, G.P. Kulbisky, Low wall shear stress predominates at sites of abdominal aortic aneurysm rupture, J. Vasc. Surg. 63 (6) (2016) 1613–1619, https://doi.org/10.1016/j.jvs.2015.01.040.

[56] M.A. Boniforti, L. Di Bella, R. Magini, On the role of hemodynamics in predicting rupture of the abdominal aortic aneurysm, J. Zhejiang Univ. - Sci. 22 (12) (2021) 957–978, https://doi.org/10.1631/jzus.A2100308.

[57] A. Arzani, G.Y. Suh, R.L. Dalman, S.C. Shadden, A longitudinal comparison of hemodynamics and intraluminal thrombus deposition in abdominal aortic aneurysms, Am. J. Physiol. Heart Circ. Physiol. 307 (12) (2014) H1786–H1795, https://doi.org/10.1152/ajpheart.00461.2014.

[58] C. Trenti, M. Ziegler, N. Bjarnegård, T. Ebbers, M. Lindenberger, P. Dyverfeldt, Wall shear stress and relative residence time as potential risk factors for abdominal aortic aneurysms in males: a 4D flow cardiovascular magnetic resonance case–control study, J. Cardiovasc. Magn. Reson. 24 (1) (2022) 1–12, https://doi.org/10.1186/s12968-022-00848-2.

[59] B. Teng, Z. Zhou, Y. Zhao, Z. Wang, Combined curvature and wall shear stress analysis of abdominal aortic aneurysm: an analysis of rupture risk factors, Cardiovasc. Intervent. Radiol. 45 (6) (2022) 752–760, https://doi.org/10.1007/s00270-022-03140-z.

[60] P. Komutrattananont, P. Mahakkanukrauh, S. Das, Morphology of the human aorta and age-related changes: anatomical facts, Anat. Cell Biol. 52 (2) (2019) 109–114, https://doi.org/10.5115/ACB.2019.52.2.109. Jun.

[61] E. Cecchi, et al., Role of hemodynamic shear stress in cardiovascular disease, Atherosclerosis 214 (2) (2011) 249–256, https://doi.org/10.1016/J.ATHEROSCLEROSIS.2010.09.008. Feb.

[62] K.M. Tse, P. Chiu, H.P. Lee, P. Ho, Investigation of hemodynamics in the development of dissecting aneurysm within patient-specific dissecting aneurismal aortas using computational fluid dynamics (CFD) simulations, J. Biomech. 44 (5) (2011) 827–836, https://doi.org/10.1016/j.jbiomech.2010.12.014.

[63] J.M. Greve, et al., Allometric scaling of wall shear stress from mice to humans: quantification using cine phase-contrast MRI and computational fluid dynamics,

[64] O. Tanweer, T.A. Wilson, E. Metaxa, H.A. Riina, H. Meng, A comparative review of the hemodynamics and pathogenesis of cerebral and abdominal aortic aneurysms: lessons to learn from each other, J. Cerebrovasc. Endovasc. Neurosurg. 16 (4) (2014) 335, https://doi.org/10.7461/jcen.2014.16.4.335.

[65] H.G. Bogren, M.H. Buonocore, Blood flow measurements in the aorta and major arteries with MR velocity mapping, J. Magn. Reson. Imag. 4 (2) (Mar. 1994) 119–130, https://doi.org/10.1002/JMRI.1880040204.

[66] S.E. Maier, D. Meier, P. Boesiger, U.T. Moser, A. Vieli, Human Abdominal Aorta: Comparative Measurements of Blood Flow with MR Imaging and Multigated Doppler US, vol. 171, 1989, p. 2, https://doi.org/10.1148/RADIOLOGY.171.2.2649924. May.

[67] J.E. Moore, D.N. Ku, Pulsatile velocity measurements in a model of the human abdominal aorta under resting conditions, J. Biomech. Eng. 116 (3) (1994) 337–346, https://doi.org/10.1115/1.2895740.

[68] J.E. Moore, D.N. Ku, C.K. Zarins, S. Glagov, Pulsatile flow visualization in the abdominal aorta under differing physiologic conditions: implications for increased susceptibility to atherosclerosis, J. Biomech. Eng. 114 (3) (1992) 391–397, https://doi.org/10.1115/1.2891400.

[69] J.E. Moore, S.E. Maier, D.N. Ku, P. Boesiger, Hemodynamics in the abdominal aorta: a comparison of in vitro and in vivo measurements, J. Appl. Physiol. 76 (4) (1994) 1520–1527, https://doi.org/10.1152/JAPPL.1994.76.4.1520.

[70] J.E. Moore, C. Xu, S. Glagov, C.K. Zarins, D.N. Ku, Fluid wall shear stress measurements in a model of the human abdominal aorta: oscillatory behavior and relationship to atherosclerosis, Atherosclerosis 110 (2) (1994) 225–240, https://doi.org/10.1016/0021-9150(94)90207-0.

[71] G.H. Mostbeck, M.C. Dulce, G.R. Caputo, E. Proctor, C.B. Higgins, Flow pattern analysis in the abdominal aorta with velocity-encoded cine MR imaging, J. Magn. Reson. Imag. 3 (4) (1993) 617–623, https://doi.org/10.1002/JMRI.1880030411.

[72] E.M. Pedersen, H.W. Sung, A.C. Burlson, A.P. Yoganathan, Two-dimensional velocity measurements in a pulsatile flow model of the normal abdominal aorta simulating different hemodynamic conditions, J. Biomech. 26 (10) (1993) 1237–1247, https://doi.org/10.1016/0021-9290(93)90071-L.

[73] B.L. Langille, Arterial remodeling: relation to hemodynamics, Can. J. Physiol. Pharmacol. 74 (7) (1996) 834–841, https://doi.org/10.1139/y96-082.

[74] A. Arzani, S.C. Shadden, Transport and mixing in patient specific abdominal aortic aneurysms with Lagrangian coherent structures, ASME 2012 Summer Bioeng. Conf. SBC (2012) 9–10, https://doi.org/10.1115/SBC2012-80475. Jul. 2013.

[75] A. Arzani, S.C. Shadden, Characterizations and correlations of wall shear stress in aneurysmal flow, J. Biomech. Eng. 138 (2016) 1, https://doi.org/10.1115/1.4032056.

[76] M.J. O'Rourke, J.P. McCullough, An investigation of the flow field within patient-specific models of an abdominal aortic aneurysm under steady inflow conditions, Proc. Inst. Mech. Eng. Part H J. Eng. Med. 224 (8) (Aug. 2010) 971–988, https://doi.org/10.1243/09544119JEIM694.

[77] J. Biasetti, T.C. Gasser, M. Auer, U. Hedin, F. Labruto, Hemodynamics of the normal aorta compared to fusiform and saccular abdominal aortic aneurysms with emphasis on a potential thrombus formation mechanism, Ann. Biomed. Eng. 38 (2) (2010) 380–390, https://doi.org/10.1007/s10439-009-9843-6.

[78] C.A. Taylor, T.J.R. Hughes, C.K. Zarins, Finite element modeling of three-dimensional pulsatile flow in the abdominal aorta: relevance to atherosclerosis, Ann. Biomed. Eng. 26 (6) (1998) 975–987, https://doi.org/10.1114/1.140.

[79] C.A. Taylor, T.J.R. Hughes, C.K. Zarins, Effect of exercise on hemodynamic conditions in the abdominal aorta, J. Vasc. Surg. 29 (6) (1999) 1077–1089, https://doi.org/10.1016/S0741-5214(99)70249-1.

[80] B.T. Tang, et al., Abdominal aortic hemodynamics in young healthy adults at rest and during lower limb exercise: quantification using image-based computer modeling, Am. J. Physiol. Heart Circ. Physiol. 291 (2) (2006) 668–676, https://doi.org/10.1152/ajpheart.01301.2005.

[81] E.M.C. Kemmerling, R.A. Peattie, Abdominal aortic aneurysm pathomechanics: current understanding and future directions, Adv. Exp. Med. Biol. 1097 (2018) 157–179, https://doi.org/10.1007/978-3-319-96445-4_8.

[82] C.M. Scotti, E.A. Finol, Compliant biomechanics of abdominal aortic aneurysms: a fluid–structure interaction study, Comput. Struct. 85 (11–14) (2007) 1097–1113, https://doi.org/10.1016/J.COMPSTRUC.2006.08.041.

[83] D.F. Young, Fluid mechanics of arterial stenoses, J. Biomech. 101 (3) (Aug. 1979) 157–175, https://doi.org/10.1115/1.3426241.

[84] H.E. Salman, H.C. Yalcin, Computational modeling of blood flow hemodynamics for biomechanical investigation of cardiac development and disease, J. Cardiovasc. Dev. Dis. 8 (2) (2021) 1–27, https://doi.org/10.3390/JCDD8020014.

[85] D.N. Ku, D.P. Giddens, C.K. Zarins, S. Glagov, Pulsatile flow and atherosclerosis in the human carotid bifurcation. Positive correlation between plaque location and low and oscillating shear stress, Arteriosclerosis 5 (3) (1985) 293–302, https://doi.org/10.1161/01.atv.5.3.293.

[86] X. He, D.N. Ku, Pulsatile flow in the human left coronary artery bifurcation: average conditions, J. Biomech. Eng. 118 (1) (1996) 74–82, https://doi.org/10.1115/1.2795948.

[87] A.S. Les, et al., Quantification of hemodynamics in abdominal aortic aneurysms during rest and exercise using magnetic resonance imaging and computational fluid dynamics, Ann. Biomed. Eng. 38 (4) (2010) 1288–1313, https://doi.org/10.1007/s10439-010-9949-x.

[88] P. Di Achille, G. Tellides, C.A. Figueroa, J.D. Humphrey, A haemodynamic predictor of intraluminal thrombus formation in abdominal aortic aneurysms,

Proc. R. Soc. A Math. Phys. Eng. Sci. 470 (2014) 2172, https://doi.org/10.1098/rspa.2014.0163.

[89] H.A. Himburg, D.M. Grzybowski, A.L. Hazel, J.A. LaMack, X.M. Li, M. H. Friedman, Spatial comparison between wall shear stress measures and porcine arterial endothelial permeability, Am. J. Physiol. Heart Circ. Physiol. 286 (5 55–5) (2004) 1916–1922, https://doi.org/10.1152/ajpheart.00897.2003.

[90] S.W. Lee, L. Antiga, D.A. Steinman, Correlations among indicators of disturbed flow at the normal carotid bifurcation, J. Biomech. Eng. 131 (6) (2009) 1–7, https://doi.org/10.1115/1.3127252.

[91] Y. Qiu, D. Yuan, Y. Wang, J. Wen, T. Zheng, Hemodynamic investigation of a patient-specific abdominal aortic aneurysm with iliac artery tortuosity, Comput. Methods Biomech. Biomed. Eng. 21 (16) (2018) 824–833, https://doi.org/10.1080/10255842.2018.1522531.

[92] D.A. Vorp, Biomechanics of abdominal aortic aneurysm, J. Biomech. 40 (9) (2007) 1887–1902, https://doi.org/10.1016/j.jbiomech.2006.09.003.

[93] D.F. Elger, D.M. Blackketter, R.S. Budwig, K.H. Johansen, The influence of shape on the stresses in model abdominal aortic aneurysm, J. Biomech. Eng. 118 (3) (1996) 326–332, https://doi.org/10.1115/1.2796014.

[94] M.S. Sacks, D.A. Vorp, M.L. Raghavan, M.P. Federle, M.W. Webster, In vivo three-dimensional surface geometry of abdominal aortic aneurysms, Ann. Biomed. Eng. 27 (4) (1999) 469–479, https://doi.org/10.1114/1.202.

[95] D.A. Vorp, M.L. Raghavan, M.W. Webster, Mechanical wall stress in abdominal aortic aneurysm: influence of diameter and asymmetry, J. Vasc. Surg. 27 (4) (1998) 632–639, https://doi.org/10.1016/S0741-5214(98)70227-7.

[96] J.P. Vande Geest, D.H.J. Wang, S.R. Wisniewski, M.S. Makaroun, D.A. Vorp, Towards a noninvasive method for determination of patient-specific wall strength distribution in abdominal aortic aneurysms, Ann. Biomed. Eng. 34 (7) (2006) 1098–1106, https://doi.org/10.1007/S10439-006-9132-6.

[97] T. Hatakeyama, H. Shigematsu, T. Muto, Risk factors for rupture of abdominal aortic aneurysm based on three-dimensional study, J. Vasc. Surg. 33 (3) (2001) 453–461, https://doi.org/10.1067/MVA.2001.111731.

[98] F.A. Lederle, et al., Rupture rate of large abdominal aortic aneurysms in patients refusing or unfit for elective repair, JAMA 287 (22) (2002) 2968–2972, https://doi.org/10.1001/JAMA.287.22.2968.

[99] P.M. Brown, D.T. Zelt, B. Sobolev, J.W. Hallett, Y. Sternbach, The risk of rupture in untreated aneurysms: the impact of size, gender, and expansion rate, J. Vasc. Surg. 37 (2) (Feb. 2003) 280–284, https://doi.org/10.1067/MVA.2003.119.

[100] J. Stenbaek, B. Kalin, J. Swedenborg, Growth of thrombus may be a better predictor of rupture than diameter in patients with abdominal aortic aneurysms, Eur. J. Vasc. Endovasc. Surg. 20 (5) (Nov. 2000) 466–469, https://doi.org/10.1053/EJVS.2000.1217.

[101] J. Biasetti, F. Hussain, T. Christian Gasser, Blood flow and coherent vortices in the normal and aneurysmatic aortas: a fluid dynamical approach to intraluminal thrombus formation, J. R. Soc. Interface 8 (63) (2011) 1449–1461, https://doi.org/10.1098/rsif.2011.0041.

[102] M. Okano, Y. Yoshida, Junction complexes of endothelial cells in atherosclerosis-prone and atherosclerosis-resistant regions on flow dividers of brachiocephalic bifurcations in the rabbit aorta, Biorheology 31 (2) (1994) 155–161, https://doi.org/10.3233/BIR-1994-31203.

[103] P.N. Watton, N.B. Raberger, G.A. Holzapfel, Y. Ventikos, Coupling the hemodynamic environment to the evolution of cerebral aneurysms: computational framework and numerical examples, J. Biomech. Eng. 131 (10) (2009) 1–14, https://doi.org/10.1115/1.3192141.

[104] N. Bappoo, et al., Low shear stress at baseline predicts expansion and aneurysm-related events in patients with abdominal aortic aneurysm, Circ. Cardiovasc. Imaging 14 (12) (2021) 1112–1121, https://doi.org/10.1161/CIRCIMAGING.121.013160.

[105] B. Ene-Iordache, A. Remuzzi, Disturbed flow in radial-cephalic arteriovenous fistulae for haemodialysis: low and oscillating shear stress locates the sites of stenosis, Nephrol. Dial. Transplant. 27 (1) (2012) 358–368, https://doi.org/10.1093/ndt/gfr342.

[106] C.F. Dewey, S.R. Bussolari, M.A. Gimbrone, P.F. Davies, The dynamic response of vascular endothelial cells to fluid shear stress, J. Biomech. Eng. 103 (3) (1981) 177–185, https://doi.org/10.1115/1.3138276.

[107] E. Metaxa, H. Meng, S.R. Kaluvala, M.P. Szymanski, R.A. Paluch, J. Kolega, Nitric oxide-dependent stimulation of endothelial cell proliferation by sustained high flow, Am. J. Physiol. Heart Circ. Physiol. 295 (2) (2008) 736–742, https://doi.org/10.1152/ajpheart.01156.2007.

[108] M.P. Szymanski, E. Metaxa, H. Meng, J. Kolega, Endothelial cell layer subjected to impinging flow mimicking the apex of an arterial bifurcation, Ann. Biomed. Eng. 36 (10) (2008) 1681–1689, https://doi.org/10.1007/s10439-008-9540-x.

[109] M. Bonert, et al., The relationship between wall shear stress distributions and intimal thickening in the human abdominal aorta, Biomed. Eng. Online 2 (2003), https://doi.org/10.1186/1475-925X-2-18.

[110] J.J. Paszkowiak, A. Dardik, Arterial wall shear stress: observations from the bench to the bedside, Vasc. Endovasc. Surg. 37 (1) (2003) 47–57, https://doi.org/10.1177/153857440303700107.

[111] R.S. Reneman, T. Arts, A.P.G. Hoeks, Wall shear stress–an important determinant of endothelial cell function and structure–in the arterial system in vivo. Discrepancies with theory, J. Vasc. Res. 43 (3) (Aug. 2006) 251–269, https://doi.org/10.1159/000091648.

[112] D. Bluestein, et al., Intraluminal thrombus and risk of rupture in patient specific abdominal aortic aneurysm - FSI modelling, Comput. Methods Biomech. Biomed. Eng. 12 (1) (2009) 73–81, https://doi.org/10.1080/10255840802176396.

[113] B.A. Zambrano, H. Gharahi, C.Y. Lim, W. Lee, S. Baek, Association of vortical structures and hemodynamic parameters for regional thrombus accumulation in abdominal aortic aneurysms, Int. j. numer. method. biomed. eng. (2021) 1–11, https://doi.org/10.1002/cnm.3555. October.

[114] B.A. Zambrano, et al., Association of intraluminal thrombus, hemodynamic forces, and abdominal aortic aneurysm expansion using longitudinal CT images, Ann. Biomed. Eng. 44 (5) (2016) 1502–1514, https://doi.org/10.1007/s10439-015-1461-x.

[115] D.A. Vorp, et al., Association of intraluminal thrombus in abdominal aortic aneurysm with local hypoxia and wall weakening, J. Vasc. Surg. 34 (2) (Aug. 2001) 291–299, https://doi.org/10.1067/MVA.2001.114813.

[116] E. Metaxa, K. Tzirakis, N. Kontopodis, C.V. Ioannou, Y. Papaharilaou, Correlation of intraluminal thrombus deposition, biomechanics, and hemodynamics with surface growth and rupture in abdominal aortic aneurysm—application in a clinical paradigm, Ann. Vasc. Surg. 46 (2018) 357–366, https://doi.org/10.1016/j.avsg.2017.08.007.

[117] J.M. Dolan, J. Kolega, H. Meng, High wall shear stress and spatial gradients in vascular pathology: a review, Ann. Biomed. Eng. 41 (7) (2013) 1411–1427, https://doi.org/10.1007/s10439-012-0695-0.

[118] H. Meng, V.M. Tutino, J. Xiang, A. Siddiqui, High WSS or Low WSS? Complex interactions of hemodynamics with intracranial aneurysm initiation, growth, and rupture: toward a unifying hypothesis, Am. J. Neuroradiol. 35 (7) (2014) 1254–1262, https://doi.org/10.3174/ajnr.A3558.

[119] H. Chen, Y. Bi, S. Ju, L. Gu, X. Zhu, X. Han, Hemodynamics and pathology of an enlarging abdominal aortic aneurysm model in rabbits, PLoS One 13 (10) (2018) 1–11, https://doi.org/10.1371/journal.pone.0205366.

[120] K. Tzirakis, Y. Kamarianakis, E. Metaxa, N. Kontopodis, C.V. Ioannou, Y. Papaharilaou, A robust approach for exploring hemodynamics and thrombus growth associations in abdominal aortic aneurysms, Med. Biol. Eng. Comput. 55 (8) (2017) 1493–1506, https://doi.org/10.1007/s11517-016-1610-x.

[121] M.J. O'Rourke, J.P. McCullough, S. Kelly, An investigation of the relationship between hemodynamics and thrombus deposition within patient-specific models of abdominal aortic aneurysm, Proc. Inst. Mech. Eng. Part H J. Eng. Med. 226 (7) (2012) 548–564, https://doi.org/10.1177/0954411912444080.

[122] R.J. Lozowy, D.C.S. Kuhn, A.A. Ducas, A.J. Boyd, The relationship between pulsatile flow impingement and intraluminal thrombus deposition in abdominal aortic aneurysms, Cardiovasc. Eng. Technol. 8 (1) (2017) 57–69, https://doi.org/10.1007/s13239-016-0287-5.

[123] E.M. Pedersen, M. Agerbaek, I.B. Kristensen, A.P. Yoganathan, Wall shear stress and early atherosclerotic lesions in the abdominal aorta in young adults, Eur. J. Vasc. Endovasc. Surg. 13 (5) (1997) 443–451, https://doi.org/10.1016/S1078-5884(97)80171-2.

[124] L.J. Kelsey, J.T. Powell, P.E. Norman, K. Miller, B.J. Doyle, A comparison of hemodynamic metrics and intraluminal thrombus burden in a common iliac artery aneurysm, Int. j. numer. method. biomed. eng. 33 (5) (2017) 1–14, https://doi.org/10.1002/cnm.2821.

[125] M. Shojima, Magnitude and Role of Wall Shear Stress on Cerebral Aneurysm. Computational Fluid Dynamic Study of 20 Middle Cerebral Artery Aneurysms, Stroke, 2004, https://doi.org/10.1161/01.str.0000144648.89172.of.

[126] H. Meng, et al., Complex hemodynamics at the apex of an arterial bifurcation induces vascular remodeling resembling cerebral aneurysm initiation, Stroke 38 (6) (2007) 1924–1931, https://doi.org/10.1161/STROKEAHA.106.481234.

[127] A. Arzani, A.M. Gambaruto, G. Chen, S.C. Shadden, Wall shear stress exposure time: a Lagrangian measure of near-wall stagnation and concentration in cardiovascular flows, Biomech. Model. Mechanobiol. 16 (3) (2017) 787–803, https://doi.org/10.1007/s10237-016-0853-7.